Chemical Science

ROYAL SOCIETY OF CHEMISTRY

EDGE ARTICLE

View Article Online
View Journal | View Issue

Open Access Article. Published on 17 January 2023. Downloaded on 6/23/2026 7:19:53 AM. This article is licensed under a Creative Commons Attribution-NonCommercial 3.0 Unported Licence.

Check for updates

Cite this: *Chem. Sci.*, 2023, **14**, 2082

All publication charges for this article have been paid for by the Royal Society of Chemistry

Received 21st October 2022
Accepted 4th January 2023

DOI: 10.1039/d2sc05828f

rsc.li/chemical-science

# A *syn* outer-sphere oxidative addition: the reaction mechanism in Pd/Senphos-catalyzed carboboration of 1,3-enynes†

Ziyong Wang, [a] Walid Lamine, [b] Karinne Miqueu *[b] and Shih-Yuan Liu *[ab]

We report a combined experimental and computational study of Pd/Senphos-catalyzed carboboration of 1,3-enynes utilizing DFT calculations, $^{31}$P NMR study, kinetic study, Hammett analysis and Arrhenius/Eyring analysis. Our mechanistic study provides evidence against the conventional inner-sphere β-migratory insertion mechanism. Instead, a *syn* outer-sphere oxidative addition mechanism featuring a Pd-π-allyl intermediate followed by coordination-assisted rearrangements is consistent with all the experimental observations.

## Introduction

Tetra-substituted alkenes are prevalent structural motifs among bioactive compounds and natural products.[1] Representative examples include illudol, cassiabudanol A, brasilenol and tamoxifen. They also serve as synthetic intermediates for downstream functionalization.[2] However, synthesis of tetra-substituted alkenes[3] in a stereo-defined manner remains nontrivial. Among numerous methods developed to date, transition metal-catalyzed difunctionalization of alkynes[4] has exhibited remarkable efficiency owing to the simultaneous introduction of two desired units across an alkyne, an inexpensive and readily available feedstock, and therefore has continuously drawn substantial attention. In this context, transition metal-catalyzed carboboration of internal alkynes[5] allows expedient synthesis of tetra-substituted alkenyl boronates[6] which are useful precursors to stereo-defined tetra-substituted alkenes. These alkenyl boronates have long been recognized as versatile building blocks[7] for their participation in Suzuki–Miyaura cross coupling[8] and in various derivatizations.[9] The carboboration approach features a diverse combination of carbon and boron moieties and all involve *syn*-selective addition of the boron group and metal across a π-bond of an alkyne (Scheme 1a). Suginome *et al.* pioneered nickel- or palladium-catalyzed intramolecular carboboration of alkynes tethered with the chloroborane moiety.[10] Similarly, extensions to intermolecular carboboration with various carbon nucleophile sources were achieved.[11] More recently, in copper-catalyzed three-component coupling systems, carboboration has been accomplished by a copper-boryl migratory insertion process with an alkyne to give an alkenyl copper intermediate, which can then be quenched by various electrophilic carbon sources.[12] Despite these breakthroughs, regio- and diastereoselectivity issues for internal unsymmetrical alkynes remain generally challenging in stereoselective carboborations to produce tetra-substituted alkenes.[12a–e] Furthermore, enolate nucleophiles have not been demonstrated as reagents in carboboration reactions. In 2021, our group reported a new *cis*-selective enolate carboboration reaction (Scheme 1b) of internal 1,3-enynes accompanying the discovery of a new family of carbon-bound boron enolates (C–boron enolates) generated by a kinetically controlled halogen exchange between chlorocatecholborane and silylketene acetals.[13] These unquaternized C–boron enolates[14] are demonstrated to activate 1,3-enyne substrates in the presence of a $Pd^0$/Senphos ligand complex. A remarkable feature is that this transformation provides access to the highly substituted dienyl boron building blocks in high site-, regio-, and diastereoselectivity.

The consistently high selectivity of the reaction and the underexplored carbon-bound boron enolates inspired our interest in understanding the reaction mechanism. In our recently reported *trans*-hydroboration[15] and *trans*-cyanoboration[16] of 1,3-enynes catalyzed by a $Pd^0$/Senphos ligand complex, an unusual "outer-sphere" oxidative addition mechanism featuring a Pd-π-allyl intermediate is proposed.[17,18] Our initial mechanistic hypothesis was analogous (Scheme 2a): the presence of Senphos ligand **L** enables (COD)Pd($CH_2TMS$)$_2$ to reductively eliminate 1,2-bis(trimethylsilyl)-ethane to form the active $LPd^0$ species **I**,[19] which then binds to the 1,3-enyne. The resulting $LPd^0$–enyne complex **II** is then activated by the Lewis acidic C–boron enolate to furnish the outer-sphere oxidative adduct **III**. An enolate equivalent then attacks Pd-π-allyl to yield the product with concomitant regeneration of $LPd^0$ species **I**.[20] Our initial hypothesis provided

[a]*Department of Chemistry, Boston College, Chestnut Hill, Massachusetts 02467-3860, USA. E-mail: shihyuan.liu@bc.edu*

[b]*Université de Pau et des Pays de l'Adour, E2S UPPA/CNRS, Institut des Sciences Analytiques et de Physico-Chimie pour l'Environnement et les Matériaux IPREM UMR 5254, Hélioparc, 2 Avenue P. Angot, 64053 Pau Cedex 09, France. E-mail: karinne.miqueu@univ-pau.fr*

† Electronic supplementary information (ESI) available: Experimental and computational details, synthetic procedures, analytical data, NMR spectra and kinetic studies (PDF). Optimized Cartesian coordinates (*XYZ*). See DOI: https://doi.org/10.1039/d2sc05828f



© 2023 The Author(s). Published by the Royal Society of Chemistry

Open Access Article. Published on 17 January 2023. Downloaded on 6/23/2026 7:19:53 AM.
This article is licensed under a Creative Commons Attribution-NonCommercial 3.0 Unported Licence.

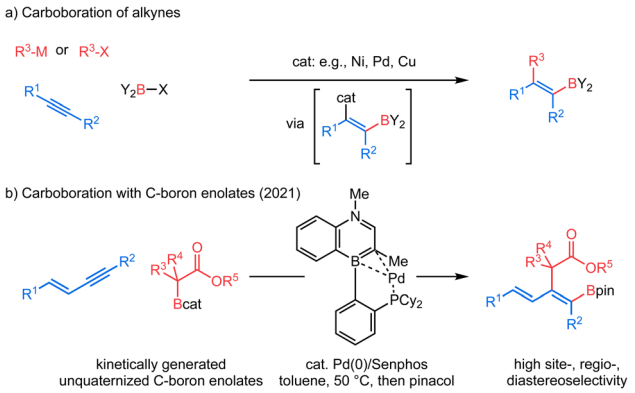


Scheme 1 Tetrasubstituted alkenyl boronates *via* carboboration reactions.

a plausible explanation for the observed high site-, regio-, and diastereoselectivity. However, many mechanistic details of the C–B bond cleavage of the C–boron enolate and the C–C and C–B bond formation in the product are vaguely defined. For example, mechanistic divergence arises as the C–boron enolate could potentially approach the LPd$^0$–enyne complex **II** either from the same side with respect to the Pd complex ("*syn*" outer-sphere oxidative addition) or from the opposite side ("*anti*" outer-sphere oxidative addition, Scheme 2b). In addition, the conventional "inner-sphere" oxidative addition[21]/β-migratory insertion/reductive elimination sequence (Scheme 2c) could not be ruled out completely, calling for new mechanistic evidence. We believe a detailed mechanistic investigation is therefore critical to clarify this mechanistic puzzle as well as to understand the origin of the selectivity and the behavior of carbon-bound boron enolates. In this article, we report our mechanistic study, starting with computational investigation (DFT calculations) which has been well correlated with $^{31}$P NMR study, kinetic study, Hammett analysis, Arrhenius analysis and Eyring analysis to obtain a more complete picture. Our mechanistic analysis does not support the inner-sphere mechanism and instead offers compelling evidence for Pd-π-allyl intermediacy as well as reveals full details for each elementary step of the new catalytic cycle, including a series of coordination-assisted rearrangements. Additionally, we also compare the ligand performance of Senphos and its carbonaceous version to probe the intrinsic effect of BN/CC isosterism. Collectively, the fundamental insights from this work should further expand the application of the Senphos ligand toward new reaction development.

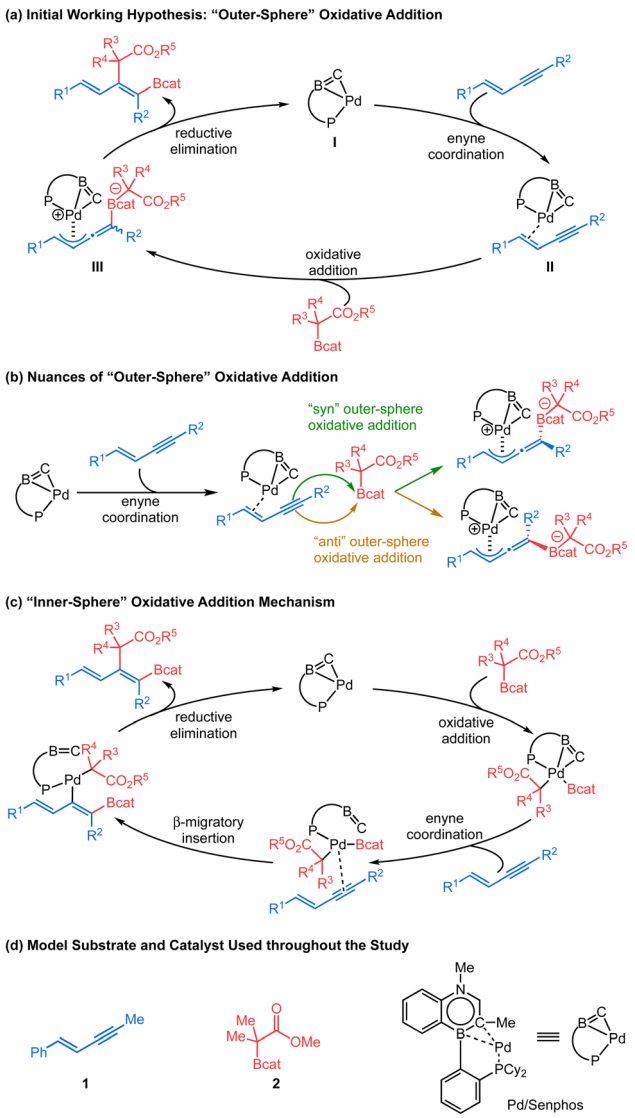


Scheme 2 Mechanistic consideration.

## Results and discussion

We selected **1** and **2** as model substrates (Scheme 2d) and performed DFT calculations to explore the mechanism at the SMD(toluene)-TPSS-D3(BJ)/SDD+f(Pd), 6-31G**(other atoms) level of theory (see the ESI† for Computational details).[22,23] Given the observed selectivity of the reaction, different pathways leading to the *cis*-addition product have been considered theoretically. We first studied the inner-sphere mechanism involving direct oxidative addition of the C–boron enolate to the Pd(0)/Senphos complex. Upon oxidative addition, two approaches of the C–boron enolate were considered leading to two products, with the Bcat moiety *cis* (path Ia, Fig. 1, **Ia-Int$_1$**) or *trans* (see path Ib, **Ib-Int$_1$** Fig. S1 in ESI†) to the phosphorus atom of the Pd(II)/Senphos complex. Then, the 1,3-enyne coordinates to the Pd(II)/Senphos complex to form **Ia-Int$_2$**. Compared to the initial reactants, this π-complex (**Ia-Int$_2$**) is strongly uphill in energy (path Ia, Fig. 1, $\Delta G$: 40.9 kcal mol$^{-1}$; path Ib, Fig. S1, $\Delta G$: 36.5 kcal mol$^{-1}$ (see the ESI)†), which may be due in part to the loss of the $\eta^2$-BC coordination of the Senphos ligand on Pd and to unfavorable steric interactions induced by the coordination of the enyne. Consequently, the β-migratory insertion, which is the rate-determining step, proceeds with an inaccessible activation barrier computed at 41.8 kcal mol$^{-1}$ for path Ia (Fig. 1) and 38.2 kcal mol$^{-1}$ for path Ib (see the ESI†). Lastly, the activation barrier for the reductive elimination is energetically less demanding ($\Delta G^{\ddagger}$: 18.7 kcal mol$^{-1}$ from starting materials, path Ia (Fig. 1); $\Delta G^{\ddagger}$: 32.8 kcal mol$^{-1}$, path Ib (see the ESI†)) than the β-migratory insertion step. Overall, the inner-sphere mechanism is predicted to be energetically

Open Access Article. Published on 17 January 2023. Downloaded on 6/23/2026 7:19:53 AM.
This article is licensed under a Creative Commons Attribution-NonCommercial 3.0 Unported Licence.

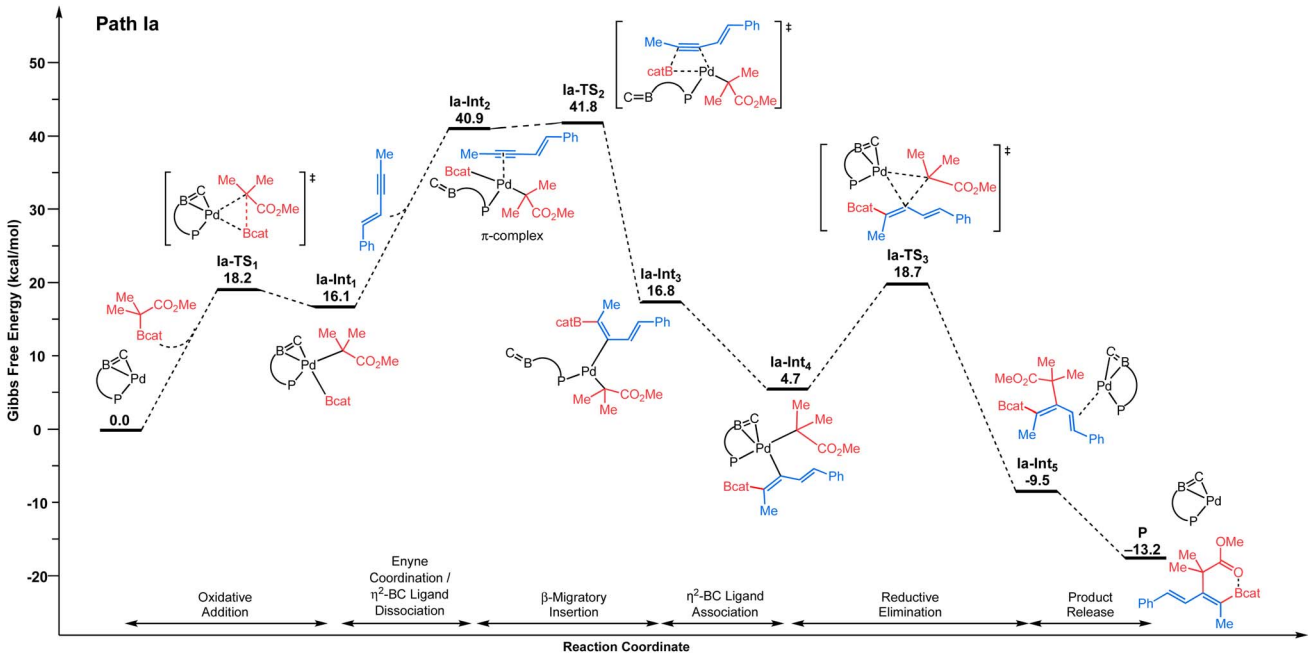


Fig. 1 Energy profile ($\Delta G$ in kcal mol$^{-1}$) computed at the SMD(toluene)-TPSS-D3(BJ)/SDD+f(Pd), 6-31G**(other atoms) level of theory for the inner-sphere mechanism involving direct oxidative addition pathway of the C–boron enolate to Pd. Path Ia is shown: Bcat moiety *cis* to phosphorus of the 1,4-azaborine-Senphos ligand. For Path Ib: Bcat moiety *trans* to phosphorus of the 1,4-azaborine-Senphos ligand, see the ESI.†

unfeasible and is not consistent with the reported relatively mild catalytic *cis*-carboboration reaction conditions.[13]

We then examined the outer-sphere oxidative addition mechanism (Scheme 2a and b), where the palladium center is not directly involved in the cleavage of the C–B bond of the C–boron enolate. As illustrated in Fig. 2, this mechanism starts with the enyne coordinating to the palladium center. The C=C double bond of the enyne is coordinated in a quasi-symmetric fashion to the metal center (Pd···C distances: 2.183–2.202 Å).[24] The formation of the π-complex (Pd–enyne) is thermodynamically favorable by 19.1 kcal mol$^{-1}$ compared to the initial reactants. Then, the C–boron enolate approaches this π-complex in a fashion *syn* to the Pd to engage in a *syn* outer-sphere oxidative addition (see the ESI† for details of the *anti* outer-sphere oxidative addition). Calculations predict that the activation barrier for the *syn* outer-sphere oxidative addition step is $\Delta G^{\ddagger}$: 16.2 kcal mol$^{-1}$ from the Pd–enyne π-complex. The "activated" quaternized C–boron enolate in **Int$_1$** then undergoes a coordination-assisted (Pd···O distance: 2.138 Å in the transition state TS$_2$) rearrangement to form a Pd–O-enolate (**Int$_2$**) with an activation barrier of 22.8 kcal mol$^{-1}$ from the resting state. This coordination assistance in the *syn* outer-sphere oxidation pathway is responsible for a 17.2 kcal mol$^{-1}$ lower overall rate-limiting energy barrier in comparison to the *anti* outer-sphere oxidative addition (or 25.1 kcal mol$^{-1}$ lower energy barrier when directly comparing the C–B bond breaking step, see the ESI† for the *anti* energy profile). The O→Pd bonding in TS$_2$ is apparent in the NBO analysis (see the ESI†) as donor–acceptor interactions with a total stabilizing energy $\Delta E(2)$ of 43.9 kcal mol$^{-1}$ ($\sum$O→Pd interaction). The natural localized molecular orbital (NLMO) associated with the main $n_O$→Pd interaction shows a major contribution of the oxygen lone pair (77%) mixed with contributions from Pd (5.3%).

From **Int$_2$**, a direct reductive elimination transition state (TS-concerted, green path, Fig. 2) *via* a concerted 5-membered transition state (Pd–O distance: 2.373 Å and C···C distance: 2.477 Å) has been located with a barrier of $\Delta G^{\ddagger}$: 59.1 kcal mol$^{-1}$ from the resting state, suggesting that this C–C bond-forming step is unlikely to take place under the relatively mild reaction conditions. Thus, an isomerization was considered before the reductive elimination step. Two possibilities were examined: (1) Pd–O-enolate to Pd–C-enolate isomerization (blue path, Fig. 2), and (2) Pd–O-enolate to B–O-enolate isomerization (black path, Fig. 2). From the resting state, the barrier for the Pd–O-enolate to Pd–C-enolate isomerization to furnish Int–Pd–C-enolate (blue) was found to be $\Delta G^{\ddagger}$: 54.4 kcal mol$^{-1}$ whereas Pd–O-enolate to B–O-enolate isomerization (black) to form **Int$_3$** is predicted to be barrierless.

From the isomerized B–O-enolate **Int$_3$**, "reductive elimination" proceeds with an activation barrier of $\Delta G^{\ddagger}$: 12.5 kcal mol$^{-1}$, leading to **Int$_4$**, which is the *cis*-carboboration product bound to the Pd catalyst. Finally, the *cis*-carboboration product is released from the Pd catalyst, and a new cycle can begin. The *cis*-carboboration product features an O→B interaction (B···O distance: 1.662 Å), in agreement with the observed $^{11}$B NMR signal of the product at 17 ppm.

Based on the computational study, the most favorable pathway to form the *cis*-carboboration product involves: (i) a *syn* outer-sphere oxidative addition, (ii) coordination-assisted B–C bond cleavage to form a Pd–O-enolate, (iii) Pd–O-enolate to B–O-enolate isomerization, and (iv) reductive elimination *via* an enolate attack to a Pd-π-allyl species. Overall, DFT calculations predict the Pd–enyne complex (Pd–enyne) to be the resting state and the reductive


© 2023 The Author(s). Published by the Royal Society of Chemistry

Open Access Article. Published on 17 January 2023. Downloaded on 6/23/2026 7:19:53 AM.
This article is licensed under a Creative Commons Attribution-NonCommercial 3.0 Unported Licence.

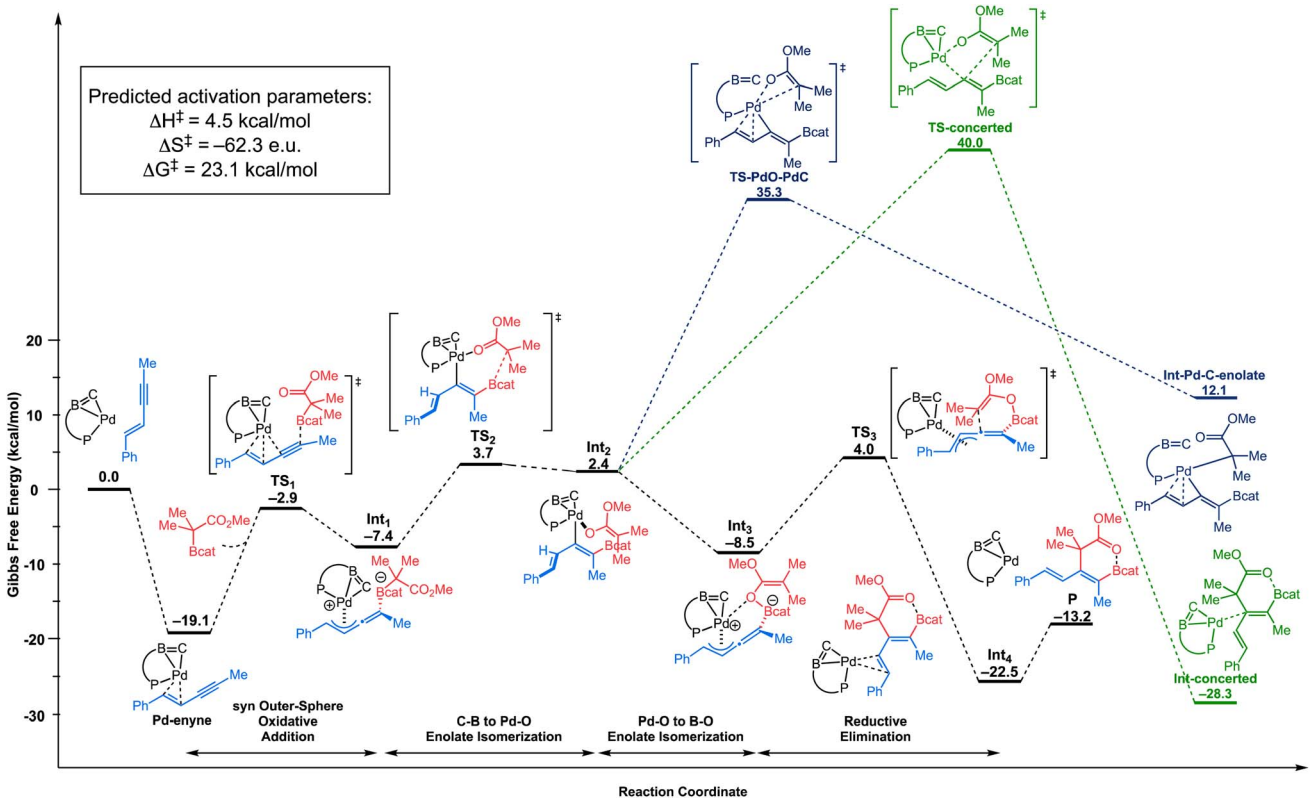


Fig. 2 Energy profiles (Δ*G* in kcal mol$^{-1}$) computed at the SMD(toluene)-TPSS-D3(BJ)/SDD+f(Pd), 6-31G** (other atoms) level of theory for the outer-sphere oxidative addition mechanism, involving B–C bond cleavage with assistance of O→Pd interaction, Pd–O/B–O isomerization and reductive elimination (black path). Concerted reductive elimination (green path), and Pd–O/Pd–C isomerization prior to reductive elimination (blue path) were also considered.

elimination ($TS_3$) to be the rate-limiting step with an overall rate-limiting barrier of 23.1 kcal mol$^{-1}$. It is worth noting that $TS_2$ (B–C to Pd–O isomerization, overall barrier of 22.8 kcal mol$^{-1}$ from the resting state) is very close in energy with $TS_3$.[25] The assistance of an O→Pd interaction between the $CO_2Me$ moiety and the Pd metal center in the *syn* outer-sphere oxidative addition pathway is critical in lowering the overall activation barrier to allow for sufficient reactivity under mild conditions.[26]

To validate the conclusion of the computational study, we performed the following experimental studies: (1) resting state determination *via* $^{31}$P NMR, (2) initial-rate kinetics to obtain reaction orders of the reactants and the catalyst, (3) Hammett analysis, and (4) determination of activation parameters. We began with $^{31}$P NMR characterization of the reaction mixture to determine the likely resting state of the catalyst. The toluene-$d_8$ solution of a 1 : 1 mixture of (COD)Pd($CH_2TMS$)$_2$ and **L** showed two broad signals ($\delta_P$ = 53.2 and $\delta_P$ = 33.3 ppm) and one sharp signal ($\delta_P$ = 52.7 ppm) (Scheme 3A). Next, the addition of 20 equiv. of enyne **1** to this solution, as a simulation of real catalytic reaction conditions, resulted in the observation of a sharp resonance ($\delta_P$ = 39.9 ppm, Scheme 3B), which we tentatively assign as the enyne-bound Pd complex (Pd–enyne). On the other hand, the addition of 40 equivalents of C–boron enolate **2** to a 1 : 1 mixture of the Pd precursor and **L** generated three additional signals ($\delta_P$ = 66.0, $\delta_P$ = 43.1, and $\delta_P$ = 38.5 ppm) with two broad signals remaining as major peaks (Scheme 3C). Under standard conditions for the catalytic reaction, the $^{31}$P NMR spectrum exhibited a major sharp peak ($\delta_P$ = 40.4 ppm) that matches nicely the signal observed for the enyne bound Pd π-complex (Scheme 3D). This peak persisted

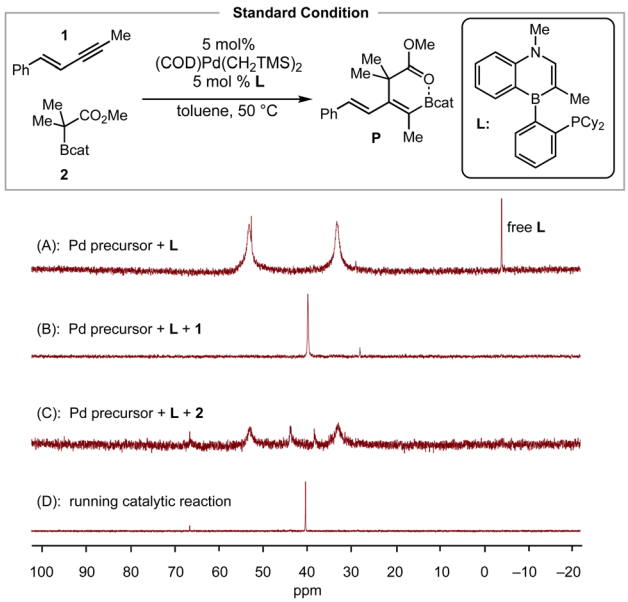


Scheme 3 $^{31}$P NMR experiments for the detection of the resting state of the catalyst.

Open Access Article. Published on 17 January 2023. Downloaded on 6/23/2026 7:19:53 AM. This article is licensed under a Creative Commons Attribution-NonCommercial 3.0 Unported Licence.

throughout the course of the reaction for *ca.* 4 hours and disappeared when the starting material was consumed. Thus, the observed $^{31}$P data are consistent with the Pd–enyne being the resting state of the catalytic cycle, which is in agreement with the DFT calculations (Fig. 2).

To probe the effect of each reaction component on the catalytic reaction, we then determined the kinetic orders in 1,3-enyne [**1**], C–boron-enolate [**2**] and [Pd/$L_{total}$], by measuring the initial rate over time in toluene-$d_8$ solutions *via* $^1$H NMR spectroscopy. Plotting the log(−d[**1**]/d*t*) *vs.* log([**2**]) (Scheme 4A), log(−d[**1**]/d*t*) *vs.* log([Pd/$L_{total}$]) (Scheme 4B) fitted two lines with slope 1.00 and 1.01, respectively, implying first order dependence on both C–boron-enolate [**2**] and [Pd/$L_{total}$]. Varying the concentration of enyne [**1**] did not influence the reaction rate (Scheme 4C), suggesting saturation kinetics (zero order dependence) with respect to [**1**]. Together with the conclusions from the $^{31}$P NMR study, the reaction order determination is consistent with the proposed *syn* outer-sphere oxidative addition pathway in Fig. 2 where the Pd–enyne complex is the resting state and the B–C bond cleavage ($TS_2$) and/or reductive elimination ($TS_3$) is the rate-limiting transition state.

We then investigated the electronic effect of the aryl group in the 1,3-enyne on the reaction rate of the carboboration (Scheme 5). The Hammett analysis reveals that a 1,3-enyne bearing an electron-donating substituent reacts faster than an unsubstituted 1,3-enyne. A linear fit with reported $\sigma_p^+$ constants is

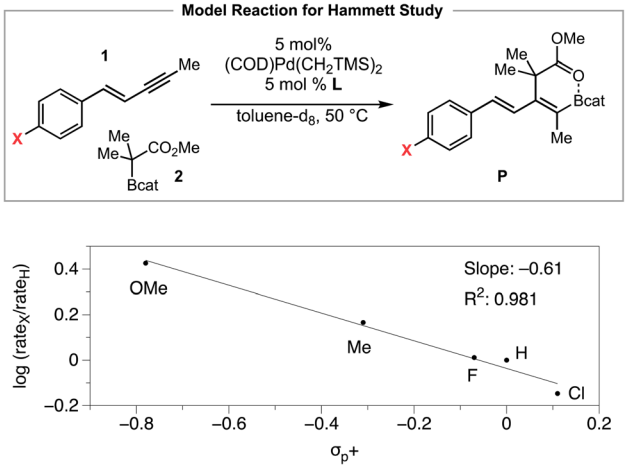


Scheme 5 Hammett analysis.

observed whereas less linear fit was obtained with $\sigma_p$ or $\sigma_p^-$ constants, respectively.[27] The $\rho$ value determined from the Hammett plot (from $\sigma_p^+$ values) was −0.61, implying the development of some positive charge in the 1,3-enyne substrate during the transition from the resting state to the rate-limiting transition state. Considering the multiple elementary processes involved (*i.e.*, see Fig. 2, (i) *syn* outer-sphere oxidative addition (developing positive charge), (ii) coordination-assisted B–C bond cleavage to form a Pd–O-enolate (reduction of positive charge), (iii) Pd–O-enolate to B–O-enolate isomerization (development of positive charge)), and (iv) reductive elimination (reduction of positive charge), the relatively small magnitude of

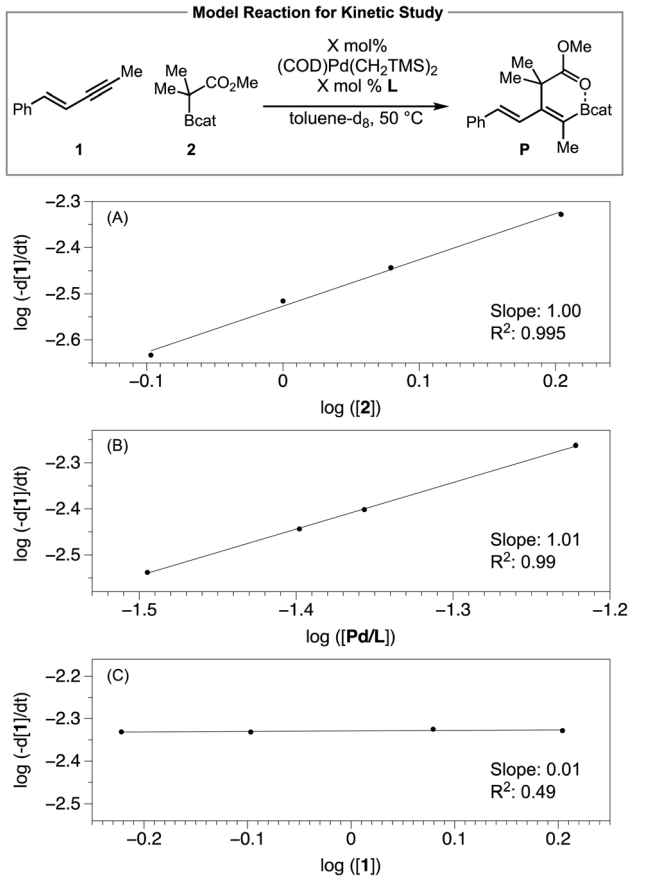


Scheme 4 Initial-rate kinetic analysis.

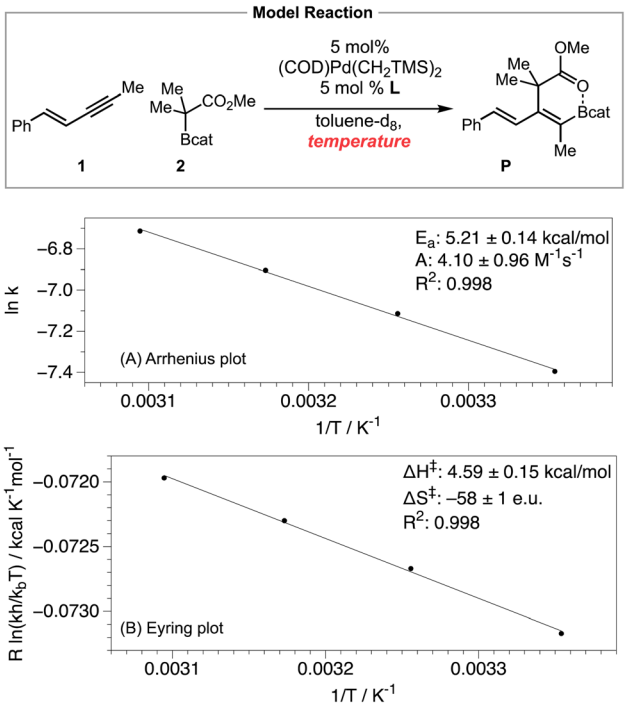


Scheme 6 Arrhenius and Eyring analysis.


© 2023 The Author(s). Published by the Royal Society of Chemistry

Open Access Article. Published on 17 January 2023. Downloaded on 6/23/2026 7:19:53 AM. This article is licensed under a Creative Commons Attribution-NonCommercial 3.0 Unported Licence.

the $\rho$ value could be interpreted as a net result of these opposing charge-generating processes.

We also obtained the activation parameters of the carboboration by measuring the reaction rate in the temperature range of 25–50 °C. The Arrhenius plot (Scheme 6A) exhibited excellent linearity, with activation energy $E_a = 5.21 \pm 0.14$ kcal mol$^{-1}$, and preexponential factor $A = 4.10 \pm 0.96$ M$^{-1}$ s$^{-1}$. Such a relatively small $A$ value is consistent with a quite negative activation entropy for this reaction.[28] We also performed an Eyring analysis (Scheme 6B) while acknowledging that the Eyring equation is theoretically only applicable to a single-step elementary reaction.[29] The activation parameters determined *via* Eyring analysis are $\Delta H^{\ddagger} = 4.59 \pm 0.15$ kcal mol$^{-1}$, $\Delta S^{\ddagger} = -58 \pm 1$ e.u., and $\Delta G^{\ddagger} = 23.25 \pm 0.22$ kcal mol$^{-1}$. While the exact values of the activation parameters should be interpreted with caution, the magnitude of the activation parameters is consistent with the prediction from the computational study (see Fig. 2, predicted $\Delta H^{\ddagger} = 4.5$ kcal mol$^{-1}$, $\Delta S^{\ddagger} = -62.3$ e.u., and $\Delta G^{\ddagger} = 23.1$ kcal mol$^{-1}$).

Achieving the rate-limiting transition state $TS_3$ from the Pd–enyne resting state involves a bimolecular outer-sphere oxidative addition step and a highly conformationally organizing reductive elimination step. The very limited degrees of freedom in the rate-limiting $TS_3$ (or in the energetically similar $TS_2$) relative to the resting state are consistent with the predicted and experimentally observed Arrhenius preexponential factor $A$ and activation entropy $\Delta S^{\ddagger}$ values.

Finally, we compared the performance of Senphos (**L**) and its carbonaceous version ($\mathbf{L_{CC}}$ ligand) under otherwise identical conditions by following the disappearance of the 1,3-enyne substrate over time *via* $^1$H NMR analysis. As can be seen from Scheme 7, the initial rate of the reaction is similar when either the **L** (BN) or $\mathbf{L_{CC}}$ ligand is used. However, the reaction stopped at ~50% conversion after *ca.* 1.5 hours when the $\mathbf{L_{CC}}$ ligand was employed while the Senphos **L** ligand enabled the reaction to go to completion over a period of 4 hours.

The 4 hours reaction time correlates with the duration of where the corresponding resting-state Pd–enyne signal is observed by $^{31}$P NMR (see the ESI†). These results suggest that the Senphos ligand **L** generates a more long-lived Pd/**L** catalyst than the $\mathbf{L_{CC}}$ ligand does and is consistent with the proposed unique $\kappa^2$, $\eta^2$-BC coordination mode of the ligand and the electron-donating borataalkene electronic structure of the BN-heterocyclic portion of the Senphos ligand.[30,31]

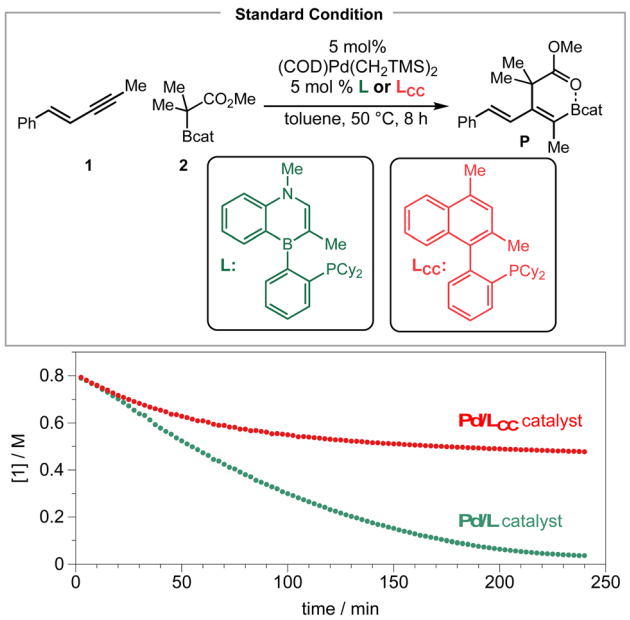


Scheme 7 BN *vs.* CC: ligand performance comparison.

## Conclusion

We have conducted a combined experimental and computational mechanistic investigation of the Pd/Senphos-catalyzed stereoselective carboboration reaction of internal 1,3-enynes with C–boron enolates. DFT calculations, spectroscopic characterization of reaction intermediates, initial-rate kinetics, linear free energy relationship analysis, and Arrhenius/Eyring analysis are inconsistent with an inner-sphere mechanism that is initiated by an oxidative addition of the C–boron enolates to the Pd(0)/**L** catalyst followed by alkyne β-migratory insertion and reductive elimination. Instead, our experimental and computational results are consistent with an outer-sphere oxidative addition mechanism where a Pd(0)/**L**–enyne complex is cooperatively activated by the Lewis acidic C–boron-enolate to furnish a zwitterionic Pd(II)/**L** π-allyl species. In contrast to the previously reported outer-sphere oxidative addition mechanism for the *trans*-selective hydroboration reaction where the Lewis acidic H-Bcat activator approaches the enyne *anti* to the Pd complex, the C–boron enolate activator approaches the enyne *syn* to the Pd complex. This *syn* outer-sphere oxidative addition pathway enables a critical coordination assisted rearrangement to form a Pd–O-enolate which then further rearranges to a B–O-enolate before the product-forming reductive elimination. Due to the lack of coordination-assisted Pd–O-enolate formation, the *anti* outer-sphere oxidative addition pathway is predicted to be more unfavorable than the *syn* outer-sphere oxidative addition mechanism by 17.2 kcal mol$^{-1}$. Our experimental and computational data are consistent with the Pd–enyne complex being the resting state and the reductive elimination being the rate-determining step of the catalytic cycle. Furthermore, we establish that the BN heterocyclic Senphos ligand generates a significantly longer-lived active Pd catalyst species than its carbonaceous ligand does. Overall, this work highlights the mechanistic nuances associated with the emerging outer-sphere oxidative addition mechanism to leverage the versatile Pd-π-allyl intermediate for new catalytic bond-forming reactions. We also hope to take advantage of the stabilizing ability of the Senphos ligand family to develop new efficient catalytic processes.

## Data availability

The data underlying this study are available in the published article and its ESI.†

© 2023 The Author(s). Published by the Royal Society of Chemistry

Open Access Article. Published on 17 January 2023. Downloaded on 6/23/2026 7:19:53 AM. This article is licensed under a Creative Commons Attribution-NonCommercial 3.0 Unported Licence.

## Author contributions

Z. W. performed the experimental mechanistic work guided by S.-Y. L. W. L. performed the computational work guided by K. M. All authors discussed the experiments and contributed to the writing of the manuscript and the ESI.

## Conflicts of interest

The authors declare no competing financial interest.

## Acknowledgements

Research reported in this publication was supported by the National Institute of General Medical Sciences of the National Institutes of Health under Award Number R01GM136920, the Excellence Initiative of Université de Pau et des Pays de l'Adour I-Site E2S UPPA, and by Boston College start-up funds. The "Direction du Numérique" of the Université de Pau et des Pays de l'Adour and Mésocentre de Calcul Intensif Aquitain (MCIA) are acknowledged for supporting computational facilities. This work was also performed using HPC resources from GENCI-IDRIS (Grant 2023-[project AD010800045R1]). Z. W. was supported as a LaMattina Graduate Fellow in Chemical Synthesis. W. L. was funded as a postdoctoral fellow by I-Site E2S-UPPA. We also acknowledge the NIH-S10 (award: 1S10OD026910-01A1) and the NSF-MRI (award: CHE-2117246) for the support of Boston College's NMR facilities. We thank Prof. Anna Chrostowska and Dr Jean-Marc Sotiropoulos at UPPA for helpful discussions.

## References

1 (*a*) A. S. Levenson and V. C. Jordan, *Eur. J. Cancer*, 1999, **35**, 1628–1639; (*b*) P. Prasit, Z. Wang, C. Brideau, C. C. Chan, S. Charleson, W. Cromlish, D. Ethier, J. F. Evans, A. W. Ford-Hutchinon, J. Y. Gauthier, R. Gordon, J. Guay, M. Gresser, S. Kargman, B. Kennedy, Y. Leblanc, S. Léger, J. Mancini, G. P. O'Neill, M. Ouellet, M. D. Percival, H. Perrier, D. Riendeau, I. Rodger, P. Tagari, M. Thérien, P. Vickers, E. Wong, L. J. Xu, R. N. Young, R. Zamboni, S. Boyce, N. Rupniak, M. Forrest, D. Visco and D. Patrick, *Bioorg. Med. Chem. Lett.*, 1999, **9**, 1773–1778; (*c*) V. C. Jordan, *J. Med. Chem.*, 2003, **46**, 1081–1111; (*d*) V. C. Jordan, *J. Med. Chem.*, 2003, **46**, 883–908; (*e*) B. M. Trost, J. P. N. Papillon and T. Nussbaumer, *J. Am. Chem. Soc.*, 2005, **127**, 17921–17937; (*f*) R. B. Williams, A. Norris, C. Slebodnick, J. Merola, J. S. Miller, R. Andriantsiferana, V. E. Rasamison and D. G. I. Kingston, *J. Nat. Prod.*, 2005, **68**, 1371–1374; (*g*) K. Itami and J.-i. Yoshida, *Bull. Chem. Soc. Jpn.*, 2006, **79**, 811–824; (*h*) N. F. McKinley and D. F. O'Shea, *J. Org. Chem.*, 2006, **71**, 9552–9555; (*i*) V. C. Jordan, *Eur. J. Cancer*, 2008, **44**, 30–38; (*j*) D. Ganapathy and G. Sekar, *Org. Lett.*, 2014, **16**, 3856–3859; (*k*) A. Lai, M. Kahraman, S. Govek, J. Nagasawa, C. Bonnefous, J. Julien, K. Douglas, J. Sensintaffar, N. Lu, K.-j. Lee, A. Aparicio, J. Kaufman, J. Qian, G. Shao, R. Prudente, M. J. Moon, J. D. Joseph, B. Darimont, D. Brigham, K. Grillot, R. Heyman, P. J. Rix, J. H. Hager and N. D. Smith, *J. Med. Chem.*, 2015, **58**, 4888–4904; (*l*) S. Savage, A. McClory, H. Zhang, T. Cravillion, N.-K. Lim, C. Masui, S. J. Robinson, C. Han, C. Ochs, P. D. Rege and F. Gosselin, *J. Org. Chem.*, 2018, **83**, 11571–11576; (*m*) W. Yin, W. Liang, L. Guo, J. Lei and F. G. Qiu, *ACS Omega*, 2018, **3**, 4551–4556.

2 (*a*) H. K. Hall Jr, *Angew. Chem., Int. Ed.*, 1983, **22**, 440–455; (*b*) H. C. Kolb, M. S. VanNieuwenhze and K. B. Sharpless, *Chem. Rev.*, 1994, **94**, 2483–2547; (*c*) C. Dobler, G. M. Mehltretter, U. Sundermeier and M. Beller, *J. Am. Chem. Soc.*, 2000, **122**, 10289–10297; (*d*) Q. H. Xia, H. Q. Ge, C. P. Ye, Z. M. Liu and K. X. Su, *Chem. Rev.*, 2005, **105**, 1603–1662; (*e*) S. W. M. Crossley, C. Obradors, R. M. Martinez and R. A. Shenvi, *Chem. Rev.*, 2016, **116**, 8912–9000; (*f*) Z. Dong, Z. Ren, S. J. Thompson, Y. Xu and G. Dong, *Chem. Rev.*, 2017, **117**, 9333–9403; (*g*) S. Kraft, K. Ryan and R. B. Kargbo, *J. Am. Chem. Soc.*, 2017, **139**, 11630–11641.

3 (*a*) A. B. Flynn and W. W. Ogilvie, *Chem. Rev.*, 2007, **107**, 4698–4745; (*b*) D. S. Müller and I. Marek, *Chem. Soc. Rev.*, 2016, **45**, 4552–4566; (*c*) P. Polák, H. Váňová, D. Dvořák and T. Tobrman, *Tetrahedron Lett.*, 2016, **57**, 3684–3693; (*d*) N. Mukherjee, S. Planer and K. Grela, *Org. Chem. Front.*, 2018, **5**, 494–516.

4 (*a*) Y. Shimizu and M. Kanai, *Tetrahedron Lett.*, 2014, **55**, 3727–3737; (*b*) T. Besset, T. Poisson and X. Pannecoucke, *Eur. J. Org. Chem.*, 2015, **2015**, 2765–2789; (*c*) D. B. Huple, S. Ghorpade and R.-S. Liu, *Adv. Synth. Catal.*, 2016, **358**, 1348–1367; (*d*) S. O. Badir and G. A. Molander, *Chem*, 2020, **6**, 1327–1339; (*e*) S. E. Bottcher, L. E. Hutchinson and D. J. Wilger, *Synthesis*, 2020, **52**, 2807–2820; (*f*) W. Liu and W. Kong, *Org. Chem. Front.*, 2020, **7**, 3941–3955; (*g*) B. Gao, D. Deng, D. Huang and X. Sun, *Synthesis*, 2021, **53**, 3522–3534; (*h*) S. Ghosh, R. Chakrabortty and V. Ganesh, *ChemCatChem*, 2021, **13**, 4262–4298; (*i*) J. Li, D. He, Z. Lin, W. Wu and H. Jiang, *Org. Chem. Front.*, 2021, **8**, 3502–3524.

5 (*a*) A. Whyte, A. Torelli, B. Mirabi, A. Zhang and M. Lautens, *ACS Catal.*, 2020, **10**, 11578–11622; (*b*) J. Corpas, P. Mauleón, R. G. Arrayás and J. C. Carretero, *ACS Catal.*, 2021, **11**, 7513–7551.

6 (*a*) K. Itami, T. Kamei and J. Yoshida, *J. Am. Chem. Soc.*, 2003, **125**, 14670–14671; (*b*) M. Shimizu, C. Nakamaki, K. Shimono, M. Schelper, T. Kurahashi and T. Hiyama, *J. Am. Chem. Soc.*, 2005, **127**, 12506–12507; (*c*) S. Mannathan, M. Jeganmohan and C. H. Cheng, *Angew. Chem., Int. Ed.*, 2009, **48**, 2192–2195; (*d*) K. Endo, M. Hirokami and T. Shibata, *J. Org. Chem.*, 2010, **75**, 3469–3472; (*e*) K. Nagao, H. Ohmiya and M. Sawamura, *Org. Lett.*, 2015, **17**, 1304–1307; (*f*) S. Roscales and A. G. Csaky, *Org. Lett.*, 2015, **17**, 1605–1608; (*g*) R. Fritzemeier and W. L. Santos, *Chem.–Eur. J.*, 2017, **23**, 15534–15537; (*h*) M. Nogami, K. Hirano, M. Kanai, C. Wang, T. Saito, K. Miyamoto, A. Muranaka and M. Uchiyama, *J. Am. Chem. Soc.*, 2017, **139**, 12358–12361; (*i*) Z. J. Kuang, H. H. Chen, J. X. Yan, K. Yang, Y. Lan and Q. L. Song, *Org. Lett.*, 2018, **20**, 5153–5157; (*j*) N. Cabrera-Lobera, M. T. Quiros, W. W. Brennessel, M. L. Neidig, E. Bunuel and D. J. Cardenas, *Org. Lett.*, 2019,

 © 2023 The Author(s). Published by the Royal Society of Chemistry

Open Access Article. Published on 17 January 2023. Downloaded on 6/23/2026 7:19:53 AM. This article is licensed under a Creative Commons Attribution-NonCommercial 3.0 Unported Licence.

**21**, 6552–6556; (*k*) W. H. Guo, H. Y. Zhao, Z. J. Luo, S. Zhang and X. G. Zhang, *ACS Catal.*, 2019, **9**, 38–43; (*l*) M. Nogami, K. Hirano, K. Morimoto, M. Tanioka, K. Miyamoto, A. Muranaka and M. Uchiyama, *Org. Lett.*, 2019, **21**, 3392–3395.

7 (*a*) D. Hall, *Boronic Acids Preparation and Applications in Organic Synthesis and Medicine Preface*, 2005; (*b*) W. B. Reid, J. J. Spillane, S. B. Krause and D. A. Watson, *J. Am. Chem. Soc.*, 2016, **138**, 5539–5542.

8 N. Miyaura and A. Suzuki, *Chem. Rev.*, 1995, **95**, 2457–2483.

9 A. Fawcett, T. Biberger and V. K. Aggarwal, *Nat. Chem.*, 2019, **11**, 117–122.

10 (*a*) M. Suginome, A. Yamamoto and M. Murakami, *J. Am. Chem. Soc.*, 2003, **125**, 6358–6359; (*b*) A. Yamamoto and M. Suginome, *J. Am. Chem. Soc.*, 2005, **127**, 15706–15707; (*c*) M. Daini, A. Yamamoto and M. Suginome, *J. Am. Chem. Soc.*, 2008, **130**, 2918–2919.

11 (*a*) M. Suginome, A. Yamamoto and M. Murakami, *Angew. Chem., Int. Ed.*, 2005, **44**, 2380–2382; (*b*) M. Suginome, M. Shirakura and A. Yamamoto, *J. Am. Chem. Soc.*, 2006, **128**, 14438–14439; (*c*) M. Daini and M. Suginome, *Chem. Commun.*, 2008, 5224–5226.

12 (*a*) R. Alfaro, A. Parra, J. Aleman, J. L. G. Ruano and M. Tortosa, *J. Am. Chem. Soc.*, 2012, **134**, 15165–15168; (*b*) H. Yoshida, I. Kageyuki and K. Takaki, *Org. Lett.*, 2013, **15**, 952–955; (*c*) Y. Q. Zhou, W. You, K. B. Smith and M. K. Brown, *Angew. Chem., Int. Ed.*, 2014, **53**, 3475–3479; (*d*) H. Y. Bin, X. Wei, J. Zi, Y. J. Zuo, T. C. Wang and C. M. Zhong, *ACS Catal.*, 2015, **5**, 6670–6679; (*e*) T. Itoh, Y. Shimizu and M. Kanai, *J. Am. Chem. Soc.*, 2016, **138**, 7528–7531; (*f*) W. Su, T. J. Gong, Q. Zhang, Q. Zhang, B. Xiao and Y. Fu, *ACS Catal.*, 2016, **6**, 6417–6421; (*g*) J. Zhao and K. J. Szabo, *Angew. Chem., Int. Ed.*, 2016, **55**, 1502–1506; (*h*) A. Boreux, K. Indukuri, F. Gagosz and O. Riant, *ACS Catal.*, 2017, **7**, 8200–8204; (*i*) T. Fujihara, A. Sawada, T. Yamaguchi, Y. Tani, J. Terao and Y. Tsuji, *Angew. Chem., Int. Ed.*, 2017, **56**, 1539–1543; (*j*) J. Mateos, E. Rivera-Chao and M. Fananas-Mastral, *ACS Catal.*, 2017, **7**, 5340–5344; (*k*) B. Mun, S. Kim, H. Yoon, K. H. Kim and Y. Lee, *J. Org. Chem.*, 2017, **82**, 6349–6357; (*l*) E. Rivera-Chao and M. Fananas-Mastral, *Angew. Chem., Int. Ed.*, 2018, **57**, 9945–9949; (*m*) E. Rivera-Chao, M. Mitxelena, J. A. Varela and M. Fananas-Mastral, *Angew. Chem., Int. Ed.*, 2019, **58**, 18230–18234; (*n*) J. del Pozo, S. C. Zhang, F. Romiti, S. B. Xu, R. P. Conger and A. H. Hoveyda, *J. Am. Chem. Soc.*, 2020, **142**, 18200–18212; (*o*) Z. H. Li, L. Zhang, M. Nishiura, G. Luo, Y. Luo and Z. M. Hou, *ACS Catal.*, 2020, **10**, 11685–11692.

13 Z. Wang, J. Wu, W. Lamine, B. Li, J.-M. Sotiropoulos, A. Chrostowska, K. Miqueu and S.-Y. Liu, *Angew. Chem., Int. Ed.*, 2021, **60**, 21231–21236.

14 (*a*) A. Abiko, T. Inoue and S. Masamune, *J. Am. Chem. Soc.*, 2002, **124**, 10759–10764; (*b*) N. J. Bell, A. J. Cox, N. R. Cameron, J. S. O. Evans, T. B. Marder, M. A. Duin, C. J. Elsevier, X. Baucherel, A. A. D. Tulloch and R. P. Tooze, *Chem. Commun.*, 2004, 1854–1855; (*c*) Z. He, A. Zajdlik and A. K. Yudin, *Dalton Trans.*, 2014, **43**, 11434–11451; (*d*) E. W. H. Ng, K. H. Low and P. Chiu, *J. Am. Chem. Soc.*, 2018, **140**, 3537–3541.

15 S. M. Xu, Y. Z. Zhang, B. Li and S.-Y. Liu, *J. Am. Chem. Soc.*, 2016, **138**, 14566–14569.

16 Y. Z. Zhang, B. Li and S. Y. Liu, *Angew. Chem., Int. Ed.*, 2020, **59**, 15928–15932.

17 (*a*) Y. N. Yang, J. L. Jiang, H. Z. Yu and J. Shi, *Chem.–Eur. J.*, 2018, **24**, 178–186; (*b*) Y. Zhang, Z. Wang, W. Lamine, S. Xu, A. Chrostowska, K. Miqueu and S.-Y. Liu, *J. Org. Chem.*, 2023, jo-2022-02841d, preprint.

18 For recent examples of Pd-catalyzed functionalization of 1,3-enynes with non-boron derived electrophiles, see: (*a*) H. Tsukamoto, T. Konno, K. Ito and T. Doi, *Org. Lett.*, 2019, **21**, 6811–6814; (*b*) Q. He, L. Zhu, Z.-H. Yang, B. Zhu, Q. Ouyang, W. Du and Y.-C. Chen, *J. Am. Chem. Soc.*, 2021, **143**, 17989–17994; (*c*) B.-X. Xiao, B. Jiang, R.-J. Yan, J.-X. Zhu, K. Xie, X.-Y. Gao, Q. Ouyang, W. Du and Y.-C. Chen, *J. Am. Chem. Soc.*, 2021, **143**, 4809–4816; (*d*) Z.-L. He, Y. Zhang, Z.-C. Chen, W. Du and Y.-C. Chen, *Org. Lett.*, 2022, **24**, 6326–6330.

19 R. Takahashi, K. Kubota and H. Ito, *Chem. Commun.*, 2020, **56**, 407–410.

20 (*a*) B. M. Trost and D. L. VanVranken, *Chem. Rev.*, 1996, **96**, 395–422; (*b*) B. M. Trost and M. L. Crawley, *Chem. Rev.*, 2003, **103**, 2921–2943.

21 (*a*) C. S. Cho, T. Ohe and S. Uemura, *J. Organomet. Chem.*, 1995, **496**, 221–226; (*b*) C. S. Cho and S. Uemura, *J. Organomet. Chem.*, 1994, **465**, 85–92.

22 (*a*) D. Andrae, U. Häußermann, M. Dolg, H. Stoll and H. Preuß, *Theor. Chim. Acta*, 1990, **77**, 123–141; (*b*) A. W. Ehlers, M. Böhme, S. Dapprich, A. Gobbi, A. Höllwarth, V. Jonas, K. F. Köhler, R. Stegmann, A. Veldkamp and G. Frenking, *Chem. Phys. Lett.*, 1993, **208**, 111–114; (*c*) J. Tao, J. P. Perdew, V. N. Staroverov and G. E. Scuseria, *Phys. Rev. Lett.*, 2003, **91**, 146401; (*d*) A. V. Marenich, C. J. Cramer and D. G. Truhlar, *J. Phys. Chem. B*, 2009, **113**, 6378–6396; (*e*) S. Grimme, J. Antony, S. Ehrlich and H. Krieg, *J. Chem. Phys.*, 2010, **132**, 154104; (*f*) S. Grimme, S. Ehrlich and L. Goerigk, *J. Comput. Chem.*, 2011, **32**, 1456–1465.

23 M. J. Frisch, G. W. Trucks, H. B. Schlegel, G. E. Scuseria, M. A. Robb, J. R. Cheeseman, G. Scalmani, V. Barone, G. A. Petersson, H. Nakatsuji, X. Li, M. Caricato, A. V. Marenich, J. Bloino, B. G. Janesko, R. Gomperts, B. Mennucci, H. P. Hratchian, J. V. Ortiz, A. F. Izmaylov, J. L. Sonnenberg, D. Williams-Young, F. Ding, F. Lipparini, F. Egidi, J. Goings, B. Peng, A. Petrone, T. Henderson, D. Ranasinghe, V. G. Zakrzewski, J. Gao, N. Rega, G. Zheng, W. Liang, M. Hada, M. Ehara, K. Toyota, R. Fukuda, J. Hasegawa, M. Ishida, T. Nakajima, Y. Honda, O. Kitao, H. Nakai, T. Vreven, K. Throssell, J. A. Montgomery Jr, J. E. Peralta, F. Ogliaro, M. J. Bearpark, J. J. Heyd, E. N. Brothers, K. N. Kudin, V. N. Star-overov, T. A. Keith, R. Kobayashi, J. Normand, K. Raghava-chari, A. P. Rendell, J. C. Burant, S. S. Iyengar, J. Tomasi, M. Cossi, J. M. Millam, M. Klene, C. Adamo, R. Cammi, J. W. Ochterski, R. L. Martin, K. Morokuma,

Open Access Article. Published on 17 January 2023. Downloaded on 6/23/2026 7:19:53 AM.
This article is licensed under a Creative Commons Attribution-NonCommercial 3.0 Unported Licence.

O. Farkas, J. B. Fores-man and D. J. Fox, *Gaussian 09, Revision D.01*, Gaussian Inc., Wallingford, CT, 2009.

24 DFT calculations show that the coordination of the alkene component of the 1,3-enyne to the Pd is energetically favored by 9.1 kcal $mol^{-1}$ than the coordination of the alkyne unit, see the ESI† for details.

25 For an example of a transition metal-catalyzed reaction featuring multiple rate-limiting steps, see: S. Okumura, S. Tang, T. Saito, K. Semba, S. Sakaki and Y. Nakao, *J. Am. Chem. Soc.*, 2016, **138**, 14699–14704.

26 The carboboration reaction when conducted at room temperature under otherwise identical conditions has a half-life of *ca.* 4 hours.

27 C. Hansch, A. Leo and R. W. Taft, *Chem. Rev.*, 1991, **91**, 165–195.

28 J. E. Nicholas, *Chemical kinetics: a modern survey of gas reactions*, Halsted Press, 1976.

29 For an example of the application of the Eyring analysis to a multistep transition metal-catalyzed reaction, see: O. P. Schmidt and D. G. Blackmond, *ACS Catal.*, 2020, **10**, 8926–8932.

30 We believe that the strong $\kappa^2$, $\eta^2$-BC coordination mode of the Senphos ligand helps maintain the structure of the active Pd complex and avoids ligand dissociation and Pd black formation.

31 S. M. Xu, F. Haeffner, B. Li, L. N. Zakharov and S. Y. Liu, *Angew. Chem., Int. Ed.*, 2014, **53**, 6795–6799.


© 2023 The Author(s). Published by the Royal Society of Chemistry